Integrative Biology



PAPER



Cite this: Integr. Biol., 2018, **10**, 516

Received 12th June 2018, Accepted 23rd July 2018

DOI: 10.1039/c8ib00103k

rsc.li/integrative-biology

Directed evolution of excited state lifetime and brightness in FusionRed using a microfluidic sorter†

Premashis Manna, Da Sheng-Ting Hung, Da Srijit Mukherjee, Da Friis, Da Friis

Green fluorescent proteins (GFP) and their blue, cyan and red counterparts offer unprecedented advantages as biological markers owing to their genetic encodability and straightforward expression in different organisms. Although significant advancements have been made towards engineering the key photo-physical properties of red fluorescent proteins (RFPs), they continue to perform sub-optimally relative to GFP variants. Advanced engineering strategies are needed for further evolution of RFPs in the pursuit of improving their photo-physics. In this report, a microfluidic sorter that discriminates members of a cell-based library based on their excited state lifetime and fluorescence intensity is used for the directed evolution of the photo-physical properties of FusionRed. In-flow measurements of the fluorescence lifetime are performed in a frequency-domain approach with sub-millisecond sampling times. Promising clones are sorted by optical force trapping with an infrared laser. Using this microfluidic sorter, mutants are generated with longer lifetimes than their precursor, FusionRed. This improvement in the excited state lifetime of the mutants leads to an increase in their fluorescence quantum yield up to 1.8-fold. In the course of evolution, we also identified one key mutation (L177M), which generated a mutant (FusionRed-M) that displayed \sim 2-fold higher brightness than its precursor upon expression in mammalian (HeLa) cells. Photo-physical and mutational analyses of clones isolated at the different stages of mutagenesis reveal the photo-physical evolution towards higher in vivo brightness.

Insight, innovation, integration

Red Fluorescent Proteins (RFPs) are advantageous for live-cell imaging owing to their low optical attenuation and phototoxicity for excitation beyond 550 nm. FusionRed, an RFP optimized for high fusion efficiency, low dimerization in vivo and low cytotoxicity in cells and tissues, is dim compared to more widely-used RFPs. We developed a microfluidic flow cytometer for sorting cell-based libraries employing both fluorescence lifetime and brightness criteria and used it to (1) visualize photophysical evolution of clones, (2) increase the fluorescence quantum yield leading to improved brightness in FusionRed variants expressed in yeast cells, and (3) produce a two-fold improvement in brightness of a FusionRed variant expressed in mammalian cells, making it comparable to that of mCherry, the most widely-used RFP.

Introduction

Fluorescent proteins (FPs) have become an indispensable tool for biological and biomedical research because their genetic encodability makes them exceptional probes for tracking cellular components in specific cellular compartments. 1 Red fluorescent proteins are excited with relatively long wavelengths of visible light beyond the absorption bands of endogenous cellular constituents, so they are particularly useful for imaging of tissues and long-term imaging with minimal photo-toxicity.² This utility motivates the engineering of brighter, more photostable FPs with red-shifted emission.³⁻⁶

^a JILA, NIST and University of Colorado, Boulder, Colorado 80309, USA. E-mail: rjimenez@jila.colorado.edu

^b Department of Chemistry and Biochemistry, University of Colorado, Boulder, Colorado 80309, USA

^c BioFrontiers Institute, University of Colorado, Boulder, Colorado 80309, USA

[†] Electronic supplementary information (ESI) available: Details of the microfluidic design and manifold assembly, schematic of electronics and signal processing, comparative screening results with linear and logarithmic amplifiers, theory of frequency-domain lifetime measurements in flow cytometry, characterization of the single mutants of FR-13, sequence alignment of the FusionRed mutants etc. See DOI: 10.1039/c8ib00103k

The main drawback of RFPs is their lower brightness compared to the green and yellow FPs. The cellular brightness for time-lapse imaging of FPs depends on many factors including the extinction coefficient, fluorescence quantum yield, expression levels (controlled by chromophore maturation, protein folding and expression from the DNA to the protein level) and photostability. Most widely-used FPs have been developed by engineering the chromophore-forming residues. their immediate environment^{7,8} or dimeric interfaces⁹ combined with random mutagenesis. Several rounds of mutagenesis and selection are usually required to obtain an FP with improved properties. There is evidence that mutations in the distal regions of the β-barrel can modulate the photo-physical properties of the FPs in unique ways, e.g. through fluctuations of the β-barrel. ^{10,11} Engineering of these residues could enhance the photo-physical diversity of the library designs and facilitate the development of substantially improved, next-generation FPs. However, the effects of individual mutations are often context-dependent and co-evolve with other residues but inclusion of additional target residues increases the library size exponentially. 12 These considerations drive the need for high information-content, high-throughput cell selection methods. Conventional methods include screening on plates,8 and/or fluorescence-activated cell sorting (FACS). Methods for screening of bacterial colonies are moving towards higher information content. For example, Mizuno and coworkers used an automated imaging system to develop photoswitchable variants of Dronpa,13 and Duwe et al. screened $\sim 10^5$ colonies to isolate photoswitchable versions of enhanced GFP. 14 Also, a fluorescence lifetime imaging system was utilized to acquire a fluorescence lifetime image of an entire petri dish to determine the lifetime and brightness of individual bacterial colonies. 15 Since the fluorescence quantum yield of FPs is correlated with the fluorescence lifetime (ESI,† Fig. S1), FPs with high quantum yield and brightness can be selected. 11,15,16 A limitation of plate-based screening is that measurements on colonies average over many cells, leaving unresolved heterogeneity of photo-physical and biochemical properties at the single-cell level. This heterogeneity can be significant and critical for applications of FPs and biosensors based on them. 17,18 As an example, Arnfinnsdottir et al.'s work on heterogeneity in GFP expression in isogenic populations of P. putida elucidated how the clonal populations do not always scale to individual cellular behavior. 18 Such heterogeneities are avoided when one uses single cell FACS based methods to characterize photo-physical properties in cells.

In contrast, FACS is capable of screening $> 10^7$ member libraries with high throughput at single cell resolution. Wang et al. employed multiple rounds of FACS-based sorting of FP libraries to generate mPlum by red-shifting the emission wavelength of a DsRed variant.¹⁹ However, FACS-based selections are limited to fluorescence intensity at a few excitation/emission wavelengths. To explore the broad fitness landscape of FPs and select mutants with a diverse range of photo-physical properties, more sophisticated fluorescence-based cell sorting techniques are required. For example, fluorescence lifetime is directly proportional to the quantum yield and independent of the

expression level. Hence, increasing the fluorescence lifetime directly leads to an enhancement of quantum yield (ESI,† Section S1), and thus improved brightness if there is no or little change in the extinction coefficient. Both time and frequencydomain fluorescence lifetime measurements have been implemented into flow cytometry but the application in directing the evolution of FP libraries towards higher quantum yield has not vet been described.

Frequency-domain lifetime methods utilize sinusoidal modulation of the excitation laser at radio frequencies, resulting in fluorescence signals oscillating at the same frequency (ω) as the excitation but with a phase shift (θ) that is related to the excited state lifetime (τ) of the fluorophore:

$$\theta = \tan^{-1}(\omega \tau)$$
.

Therefore, the measurement of phase shift reveals the excited state lifetime of the fluorophore (ESI,† Section S6). Although time-domain approaches are capable of extracting the multi-exponential nature of fluorescence decay in a flow cytometric platform, 20 we use a frequency-domain technique due to its relatively higher throughput and simplicity of implementation with a commercial high-speed lock-in amplifier.

Frequency-domain flow cytometry was first demonstrated to measure fluorescence lifetimes from fluorescent beads and cells labeled with dyes, which exhibit similar emission spectra that are difficult to resolve. 21,22 Though fluorescence lifetime measurement combined with flow cytometry was mostly used for the purpose of analysis and screening in early developments, 23,24 many recent efforts have been made to incorporate sorting ability. Cao et al. used the analog method22 to sort cells and beads labeled with fluorophores with spectrally overlapping fluorescence based on the lifetime, with a priori knowledge of the fluorophore lifetimes.²⁵ This approach utilizes an intensitymodulated excitation source and requires phase sensitive detection electronics to obtain the average fluorescence lifetime. Houston and coworkers demonstrated sorting of fluorescent beads based on a digitally modulated excitation source and lifetime analysis using the frequency-domain technique modified with an open reconfigurable cytometric acquisition system capable of digital signal-processing.²⁶ Though a priori knowledge of the lifetimes of the fluorophores is not required in the digital system, the system loses out to the better signal to noise ratios seen in analog systems. Using the digital system, Sands et al. developed a method to simultaneously measure the phase delay related to the fluorescence lifetime and the emission modulation depth as an additional criterion, and demonstrated the ability to sort cells expressing isospectral FPs with differing lifetimes.²⁷ The digital technique was further developed by Yang et al. to screen two nearinfrared FPs based on lifetimes, demonstrating the ability to distinguish two FPs with similar emission intensity.²⁸ While these studies demonstrated sorting of cells containing a small set (usually two kinds) of FPs based on the fluorescence lifetime, there is no report on sorting an FP library and its applications.

We first reported a microfluidic platform capable of selecting RFP mutants with improved photostability. 29,30 In another

study, multiparameter photo-physical analysis of RFP libraries was performed to quantify the brightness, photostability and fluorescence lifetime of cell-based libraries using a custombuilt analog phase sensitive microfluidic cytometer.³¹ Here, we describe further development in combining sorting with lifetime measurements on libraries of FusionRed (abbreviated as FR), a protein developed to address the dimerization and cytotoxicity issues observed in several RFPs.9 With its reduced dimerization tendency,³² improved fusion efficiency and low cytotoxicity,⁹ FusionRed has the potential to be an excellent bio-marker for live-cell imaging, but its relatively low molecular brightness due to its low fluorescence quantum yield and low cellular brightness relative to mCherry, the most commonly used RFP, limit its attractiveness. We hypothesized that an improvement in the excited state lifetime would lead to an increase in the quantum yield of this FP, resulting in enhanced molecular brightness. We also hypothesized that the low brightness of FusionRed in cells originates from the low protein expression level since the molecular brightness of FusionRed⁹ is higher than that of mCherry. We demonstrate the use of our instrument to "watch" FusionRed clones evolving towards higher quantum yield through multiple rounds of error-prone PCR (EP-PCR) mutagenesis and selection. This process led to the generation of substantially brighter FusionRed variants. To the best of our knowledge, our work is the first to report the use of a frequencydomain flow cytometer for the directed evolution of FP lifetime, quantum yield and brightness.

Experimental section

Microfluidic design & manifold assembly

We adopted a 2D hydrodynamic focusing microfluidic design from our previous work, consisting of three inlets (sheath, sample and sheath) and two outlets (collection and waste). 29,33 Cell suspensions are flowed through the middle channel, which is focused onto a narrow stream by two sheath channels. Details of the design are given in the ESI,† Fig. S2a. The chip is sealed to a polytetrafluoroethylene (PTFE) manifold with O-rings (ESI,† Fig. S2b). Three inlets of the manifold are connected with and regulated by three pressure-controllers (Pneutronics, OEM, EPS10-5-0-2) for independent control of the flow in each channel. The inlet reservoirs of the manifold can be filled with up to 150 µl of sample or sheath buffers. The two outlets (collection and waste) are open to ambient pressure.

Optical set-up

The optical set-up for the microfluidic sorter is presented in the ESI,† Fig. S3. A 561 nm laser (Genesis MX, Coherent, 1W) beam is split with a 70:30 beam splitter. The higher power beam is directed through an electro-optic modulator (EOM, ThorLabs, EO-AM-NR-C4) that amplitude-modulates the beam at a frequency of 29.5 MHz. Before the beam enters the EOM, it is focused with a lens to fit into the EOM aperture. Two polarizers (Newport) and a half-wave plate (Newport) are used to control the power of the lifetime beam after the EOM. The lower power beam and the modulated beam pass through a 150 mm planoconvex cylindrical lens, transforming the circular beams into elliptical ones. The elliptical beams from the cylindrical lens enter the side-port of a commercial inverted microscope (Olympus IX71), reflected through a dichroic mirror (Semrock, FF573-Di01-25x36), and focused into the microfluidic chip through an air-objective (Olympus, 20×, NA 0.45). The FWHM of the lifetime beam is measured to be 9 um and 56 um in the minor and major axes of its elliptical spatial mode, respectively. The other beam has similar dimensions. Epifluorescence from cells expressing RFPs is separated from the excitation beams using a band-pass filter (Semrock, FF01-629/56-25). Subsequently, the lifetime and timing beams are spatially separated with mirrors and slits and collected by two red-wavelength sensitive photo-multiplier tubes (PMT, Hamamatsu R9880U-20) as illustrated in the ESI,† Fig. S3.

Detection electronics

The electronic components for detection, amplification and processing of fluorescence signals are schematically illustrated in the ESI,† Fig. S4. A function generator (Agilent, 33520B) is used to provide a sinusoidally modulated electrical signal with 10 V (peak-to-peak) at 29.5 MHz to drive the EOM, and also send a 1 V peak-to-peak reference signal to the lock-in amplifier. The fluorescence signal obtained from the lifetime PMT is split into two components (high and low frequencies) using a biased-tee. The high frequency component (~30 MHz) is directed to a custom-made amplifier and then sent to a lock-in amplifier (Zurich Instruments, UHF) for frequency-domain lifetime measurements. The lock-in amplifier outputs in-phase and quadrature phase signals that are used for frequency-domain measurements of the excited state lifetime of the RFP mutants. The low frequency components (<83 kHz) from the biased-tee, along with the signal from the timing beam are further amplified with a home-built trans-impedance amplifier for improving the signal-to-noise ratios. Electronic amplification of the fluorescence signal from the lifetime beam is achieved by either a linear or a logarithmic trans-impedance amplifier. The logarithmic amplifier has a higher dynamic range and thus helps in resolving the brightness of a mixture of mutants better than the linear amplifier (ESI,† Fig. S5). Finally, all the signals are digitized at 125 kHz, 16-bit resolution by a data acquisition card (DAQ, National Instruments BNC-209a, PCI-6251 with NI-SCX). The DAQ board communicates with a target computer that runs the LabView RealTime module to analyze the digitized data streams, identify the isolated non-overlapping bursts of peaks due to the passage of cells through the laser beams, and perform selection decisions based on user-defined thresholds of lifetime, fluorescence intensity or transit time of the cells. The Target computer is connected to a Host computer that controls the operation of the sorter and is used for real-time data display.

Cell culture, library generation, and sample preparation

We employ yeast (Saccharomyces cerevisiae) as the host organism for this work because we aimed to carry out a selection in eukaryotic cells rather than prokaryotic cells. Yeast cells also

offer advantages in library generation, screening, and sorting because the recovery of yeast cells after sorting is faster than mammalian cells due to their fast doubling time (~90 minutes in yeast versus ~ 20 h in HeLa cells, respectively). However, the results suggest that RFPs developed from yeast cells do not necessarily retain their performance in mammalian cells, despite both being eukaryotic cells.

For all the EP-PCR libraries described in this report, a typical error-rate is used that incorporates ~ 5 mutations (at the nucleotide level) per template. To achieve this mutation rate, 100-500 ng of initial target DNA and 30 PCR cycles are used. Typical size of the EP-PCR library is $\sim 3 \times 10^6$. Assuming the mean mutation frequency per gene as 5 and length of the template as 708 base pairs, each library contains $\sim 2 \times 10^6$ number of distinct full-length FP variants. The analysis of distinct mutants in EP-PCR libraries is based on the algorithm by Patrick et al.³⁴ Details of the library generation protocol are provided in the ESI,† Section S7.

For the microfluidic screening of yeast cells containing RFPs, the corresponding library or the culture is freshly grown from a stored stock and expressed transiently. A 0.5 ml volume of stored culture media is added to 10 ml solution of growth media (yeast nitrogen base, ammonium sulphate, dextrose) and grown for 8 h. Next, 0.5 ml of this freshly-grown cell culture is added to 10 ml solution of induction media (yeast nitrogen base, ammonium sulphate, galactose, raffinose). Cells are screened or sorted 17-20 h after induction. During growth and expression, the cultures are incubated at 30 °C and constantly shaken at 250 rpm.

For screening/sorting, yeast cells expressing the library are diluted (10-20 fold) with the blank media (yeast nitrogen base, ammonium sulphate) containing 14% OptiPrep (60% weight/ volume iodixanol in water), and subsequently filtered using a 40 µm filter to remove cell debris prior to loading into the microfluidic chip.

Multi-parametric screening

Microfluidic screening reveals the fluorescence intensity and excited state lifetime profiles of the individual mutants or RFP libraries (Fig. 2a and b). Based on the initial screening results of a library, a decision is made to sort a sub-population of the library having a significantly longer lifetime and/or higher fluorescence intensity for further enrichment and selection as described in greater detail in the Results section.

As a cell passes through the lifetime and timing beams (Fig. 1), fluorescence signals are detected by two PMTs. After signal processing (ESI,† Fig. S4), digitized data from the PMTs are analyzed by custom-made LabView software that quantifies the excited state lifetime of the mutants from the in-phase (V_I) and quadrature phase (VO) values provided by the lock-in amplifier (ESI,† Section S6).

For assessing the brightness of the mutants, the fluorescence intensity from the lifetime beam was used. During the microfluidic screening, either a linear or a logarithmic amplifier was used for the amplification of the lifetime PMT signal. Although both amplifiers clearly resolve the excited state lifetime of the

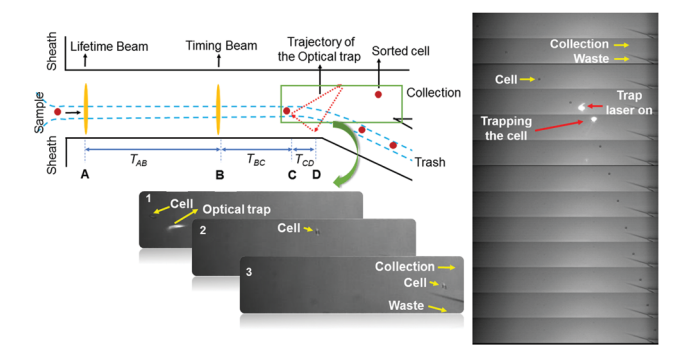


Fig. 1 (left) Sorting of improved RFP variants with optical gradient force switching. Details of the sorting procedure are described in the main text. A portion of the microfluidic is zoomed in to display a yeast cell being sorted into the collection channel. (right) The stack of images displaying multiple frames of a yeast cell in flow being sorted by the trap laser.

mutants, owing to its higher dynamic range, only the logarithmic amplifier captures the peak of the fluorescence intensity (ESI,† Fig. S5). The screening in the microfluidic setup is operated at a typical rate of ~ 30 cells per s, which optimizes the flow rates, signal processing and data storage in the current electronic and software configuration. Higher screening speeds can be achieved with faster electronics such as a field-programmable gate array (FPGA) based system.

Selection of improved fluorescent protein variants

Once the lifetime and brightness profiles of an RFP library are revealed through the microfluidic screening, the next step is to sort the mutants with desired photo-physical properties. We employ optical force gradient-based sorting that does not require a high-NA objective and is compatible with live cells. Typically, 6-8 W from a 1064 nm laser is required to generate force for cell deflection, and details relevant to the optical design of the trap laser have been discussed in a previous report by Davis et al.29

The sorting process is illustrated in Fig. 1. First, the flow is biased to direct cells into the waste channel. The trap-laser is focused onto a place close to the junction of collection and waste channels and slightly below the sample stream. The trap laser is only turned on (and moves from the lowest position of the triangle along the direction of the arrows shown in Fig. 1) after the LabView software makes a sorting decision, based on the thresholds of the desired photo-physics for the experiment. The LabView software measures the distance between A and B when the pixel positions of the lifetime and timing beams are entered. From the transit time of cells from A to B (T_{AB}) and the physical distance between them, the velocity of the cells in the microfluidic channel is computed. From the measured cell velocity and the distance from B to C and C to D, the transit time of the cell to travel BC (T_{BC}) and CD (T_{CD}) are calculated. $T_{\rm BC}$ and $T_{\rm CD}$ determine the delay time and the sweeping velocity of the trap laser so that the trap laser intercepts the cell and deflects it to the collection channel. However, the speed of the cells is not uniform in the microfluidic channel and tends to decrease in the sorting junction. To account for this effect,

another adjustable parameter (Extra Delay) was added in the software. The value of the Extra Delay parameter is optimized to increase the sorting efficiency through visual inspection of the cell trajectory in the camera. Once the sorting efficiency is optimized, mutants with improved photo-physical properties can be sorted based on user-defined thresholds.

After the enrichment of a subpopulation by microfluidics, the FP library is expressed on agar plates. Next, single mutants are picked from the plates guided by the individual colony lifetimes for further characterization. The lifetime of an individual colony was measured in a fashion similar to the in-flow phase fluorimetry. The lifetime beam (Fig. 1) was manually focused onto single colonies at a low excitation intensity to avoid saturation of the PMT. The PMT signal was demodulated by the lock-in amplifier (Zurich Instruments, UHF). The resulting in-phase and in-quadrature outputs were digitized and processed to extract fluorescence lifetime values. To verify the performance of this technique, mCherry and TagRFP-T colonies were used as references. Each plate contained ~ 200 colonies and it took ~ 30 minutes to screen the plate manually based on the fluorescence lifetime of individual colonies. If the FP libraries were plated and screened without microfluidic enrichment for the selection of mutants, it would take \sim 75 h to screen ~30 000 cells. However, automated cell/colony-picking can enhance the speed of plate-based selections.³⁵

Results

Error-prone FusionRed library

We first generated a random mutagenesis library (EP-PCR library), then subjected it to multiple rounds of multi-parametric microfluidic sorting to select the desired sub-library, followed by plating and selection of colonies based on the excited state lifetime. Fig. 2 displays the screening results of FusionRed (wild-type) and the EP-PCR library expressed in yeast. The library contained a small population (\sim 5%) with longer excited state lifetime than the

wild-type FusionRed. Three rounds of microfluidic sorting were performed to enrich this population (Fig. 2b; population in the pink box) with a selection gate: lifetime > 2.2 ns. In each round of sorting, typically ~ 2500 cells were isolated from a pool of ~ 30000 cells and grown thereafter for subsequent sorting. Following these enrichments, the library was expressed on galactose-containing plates. Approximately 20 mutants of FusionRed were selected from these plates, guided by the excited state lifetime of the colonies (Experimental section).

Out of several FR mutants selected from the lifetimeenriched libraries, the excited state lifetimes of FR-1 and FR-13 were found to be 2.5 ns and 2.8 ns (measured in microfluidic screening) respectively, which was significantly higher than the lifetime of FusionRed (2.0 ns). Though FR-1 has a shorter excited state lifetime compared to FR-13, its high cellular brightness shows its potential. Therefore, FR-1 and FR-13 were chosen as templates to engineer mutants with higher brightness. Some clones exhibit longer lifetimes but low brightness, this can be either due to reduced extinction coefficients at 561 nm excitation or poor expression of such FP mutants at the cellular level. Thus, some clones with a longer lifetime and low brightness may be a consequence of heterogeneity in expression levels.

FR-13 mutant

FR-13 was expressed and purified from E. coli and a series of photo-physical characterizations were carried out. Table 1 displays the photo-physical properties of FR-13 and FusionRed. As expected, measurements in purified protein revealed a significant increase in lifetime of FR-13 compared to FusionRed. The ~1.5-fold increase in lifetime of FR-13 correlated with an approximate ~1.8-fold enhancement of quantum yield as compared to its precursor, FusionRed. The in vitro brightness calculated from the values of $\varepsilon_{\rm max}$ and φ of this mutant is ~ 2.6 fold higher than wild-type FusionRed. The in vitro brightness of FR-13 reflects the effectiveness of selection based on the correlation between the

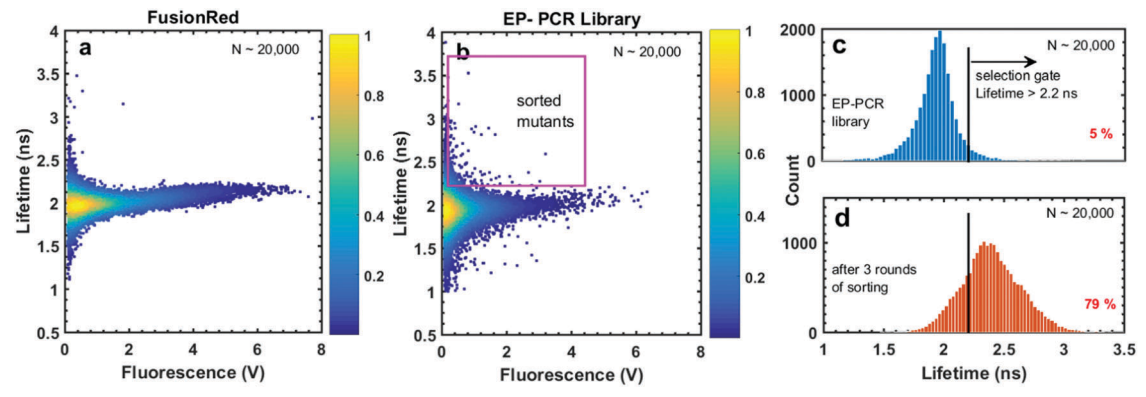


Fig. 2 Microfluidic screening dot plots displaying lifetime and brightness (fluorescence signal in volts) profiles of FusionRed (pseudocolor indicates the normalized cell counts at a certain value of brightness and lifetime on the plot – from yellow indicating the highest till indigo indicating the lowest) (a) and the FusionRed EP-PCR library (b) generated by random mutagenesis. The library contained a population with a longer lifetime (enclosed in the pink box). (c and d) The EP-PCR library was subjected to microfluidic-based sorting to enrich the population with lifetime longer than 2.2 ns. After three rounds of sorting, the percentage of the population with lifetime longer than 2.2 ns increased from 5% to 79%. The FR-13 and FR-1 mutants were selected from this lifetime-enriched population.

Table 1 Photo-physical properties of the mutants derived from FR-13. Brightness values in yeast are the mean fluorescence intensity in the cells expressing the mutants as measured by FACS (Fig. 4a). Values of λ_{abs} and λ_{em} are the maximum wavelengths of visible absorption and emission spectra, respectively, τ is the excited state lifetime, φ is the fluorescence quantum yield, and ε_{max} is the extinction coefficient at the absorption peak. Details of photo-physical measurements are described in the ESI Section S11

RFP	$\lambda_{abs} \ (nm)$	λ_{em} (nm)	τ (ns)	φ	$\varepsilon_{\text{max}} \left(\text{M}^{-1} \text{ cm}^{-1} \right)$	Molecular brightness ($\varepsilon \times \varphi$)	Brightness (in yeast)
FusionRed	575	596	1.8	0.26	87 300	100	100
FR-13	571	591	2.7	0.48	124 000	262	27
FR-F	571	591	2.6	0.36	104 000	165	138
FR-G	572	591	2.7	0.42	105 000	194	144
FR-H	572	592	2.6	0.42	90 100	167	142

excited state lifetime and quantum yield from the perspective of photo-physics. However, the brightness of FR-13 measured by FACS screening (Table 1) and microfluidic screening (Fig. 3c) in yeast showed that it was dimmer than FusionRed. These inconsistencies between in vivo and in vitro brightness of FR-13 may be attributed to its slower chromophore maturation or lower expression efficiency in yeast.

Sequencing of FR-13 revealed the following mutations relative to FusionRed: H25Y, V49I, F83Y and A224T. The amino acid residues were numbered by aligning the sequence of the FR mutants with the avGFP sequence as carried out in the original report on FusionRed.⁹ The sequence alignment is presented in the ESI,† Section S10.

To improve the in vivo brightness of FR-13, we first investigated the roles of the four mutations. Of these, only position 224 was internal (facing into the β-barrel) while others were located either in the α -helix (F83) or facing outward of the barrel (H25 & V49). We reverted the mutations individually back to the original FusionRed residues (i.e. constructed FR-13 Y25H, FR-13 I49V, FR-13 Y83F and FR-13 T224A) and performed microfluidic screening in yeast cells. We observed that the introduction of a T224A mutation in FR-13 resulted in improved brightness and reduced excited state lifetime (ESI,† Fig. S6), and therefore concluded that the longer lifetime and lower brightness of FR-13 originated solely from the A224T mutation.

These photo-physical measurements led us to hypothesize that targeting of position 224 with full saturated mutagenesis might yield FR-13 mutants with similar or higher lifetime and improved brightness. However, the site-directed libraries generated by targeting only A224 or in combination with other positions mutated in FR-13 i.e. H25, V47 & F83 did not produce variants with higher brightness or longer lifetime. We therefore turned to a random mutagenesis approach.

Multiple rounds of error-prone mutagenesis on FR-13 and subsequent microfluidic enrichment based on brightness generated three mutants (Fig. 3 and ESI,† Fig. S7) that showed improved brightness in yeast: FR-F, FR-G and FR-H. Purification of these mutants and in vitro characterization revealed higher molecular brightness (quantum yield × extinction coefficient) relative to FusionRed (Table 1). Details of the evolution of FR-13 mutants are described in the ESI,† Section S9.

FR-F, G and H mutants showed higher brightness in yeast (Fig. 4a), thus could be useful for expressing in yeast considering the advantages of FusionRed mutants. However, when they

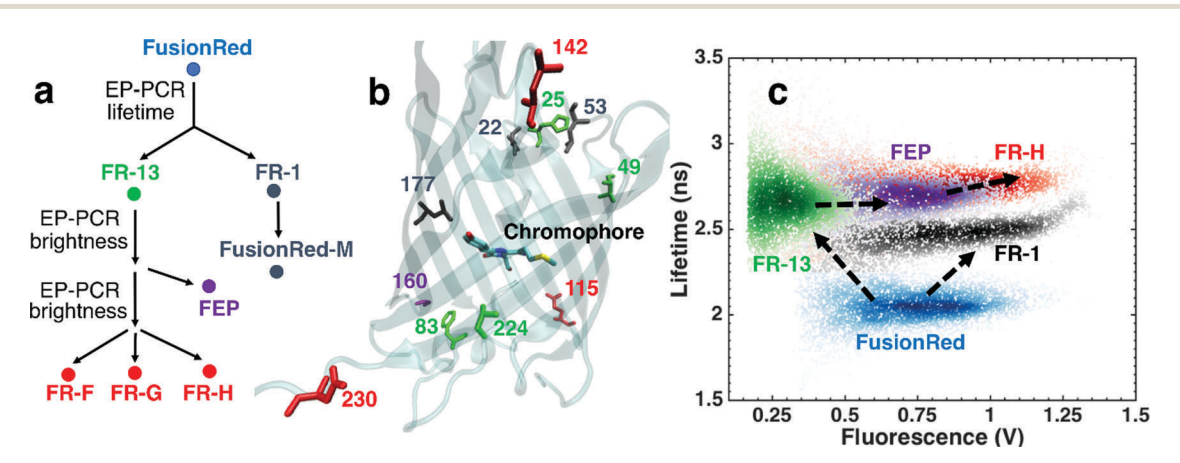


Fig. 3 Directed evolution of FusionRed: (a) genealogy of the FusionRed mutants. FR-13 was generated from the error-prone mutagenesis library of FusionRed and subsequent selection based on the excited state lifetime of the mutants. Two rounds of random mutagenesis on FR-13 and selection based on brightness produced FR-F, FR-G and FR-H mutants with improved brightness upon yeast expression, whereas one round gave the FEP mutant. In a separate evolutionary route, FusionRed-M was generated from FR-1 which showed ~2-fold higher brightness than FusionRed in a mammalian cell line. (b) Mutations introduced at the first (green), second (purple) and third rounds (red) of EP-PCR mutagenesis during the evolution of FR-13 and FR-13 mutants. Amino acid residues involved in the FR-1 mutant are displayed in black. Locations of the amino acid residues are shown in the crystal structure of mKate (PDB: 3bxb). VMD⁴⁰ was used to generate this structure. (c) Evolution trajectory of the FusionRed mutants displaying their lifetime and brightness (fluorescence signal in volts) profiles. Individual mutants were expressed in yeast and screened in the microfluidic platform with ∼5000 cells. The screening results were overlaid with different color maps to generate this plot.

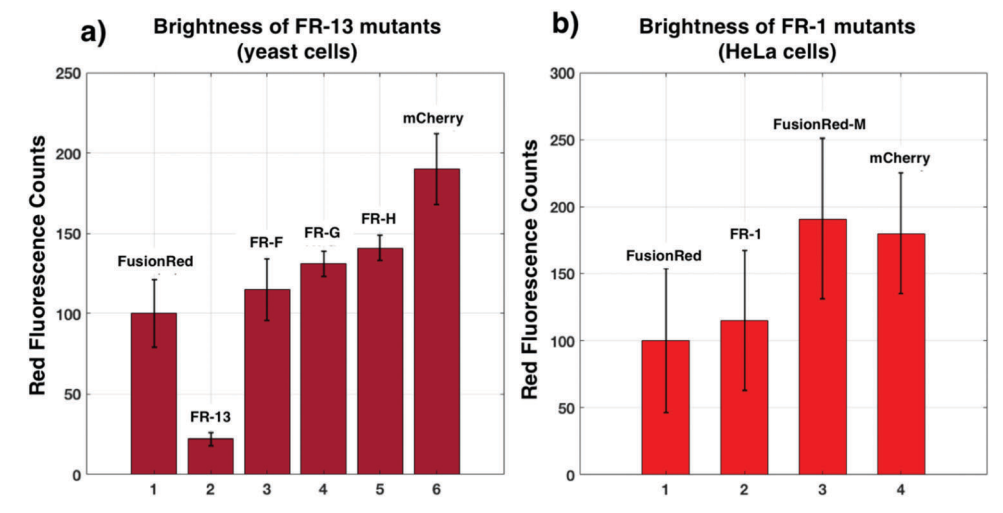


Fig. 4 Mean red fluorescence intensities averaged from three biological replicates relative to FusionRed. (a) 20 000 cells were FACS screened \sim 18 h post-induction in the cytoplasm of yeast cells for each RFP. (b) 10 000 cells were FACS screened \sim 48 h post-transfection in HeLa cell-lines (H2B-RFP constructs) for each RFP. Details are described in the ESI,† Section S12. FusionRed-M displayed \sim 2-fold higher brightness relative to its precursor FusionRed in the HeLa cell line, and FR-F, G, and H clones showed higher brightness in yeast cells compared to the precursor FR-13.

were expressed in mammalian cells, brightness was not significantly higher relative to FusionRed. Sequence analysis showed the presence of a V4M mutation in all of the mutants (ESI,† Section S10). During the evolution of mKate2 from mKate, the M4V mutation was introduced to create an optimal Kozak sequence and efficient expression in the mammalian cells.³⁶ Another study based on FACS-seq indicated that multiple initiation sites, as observed in these mutants, could be detrimental for the effective expression of the proteins in the mammalian cells.³⁷ From these analyses, we hypothesized that reversing the V4M mutations in these mutants could improve their expression efficiency and brightness in mammalian cells. Hence, we generated the FRX mutants: XF (FR-F, M4V); XG (FR-G, M4V); XH (FR-H, M4V). However, when stably expressed in MCF10A cell-lines, the brightness of these FRX mutants was lower than that of FusionRed. This inconsistency in brightness of the FRX mutants is most likely due to the lower expression efficiency or slower chromophore maturation in mammalian cells. As multiple attempts to improve the brightness of FR-13 in mammalian cell lines were unsuccessful, we focused on the FR-1 mutant.

FR-1 mutant

FR-1 was found to have a longer lifetime and higher quantum yield compared to FusionRed (Table 2). Although the *in vitro*

brightness of FR-1 was found to be only 30% higher than that of FusionRed, when expressed in yeast it showed \sim 3.5-fold higher brightness (ESI,† Section S12).

The FR-1 mutant has the following mutations relative to FusionRed: V22I, L53P and L177M. The L177 sidechain points into the β -barrel and is located close to the chromophore. On the other hand, L53 and V22 are located in the loop region (Fig. 3b). From our previous experience with FR-13 mutants, we hypothesized that due to its proximity to the chromophore, L177 may be crucial in modifying the photo-physical properties in FR-1. We therefore generated FusionRed L177M (called FusionRed-M and abbreviated as FR-M). Table 2 compares the photo-physical properties of FusionRed, FR-1 and FusionRed-M. Both FR-1 and FusionRed-M mutants have higher in vitro brightness relative to FusionRed. However, FusionRed-M performs better than FR-1 when transiently expressed in the nuclei of the HeLa cells (H2B-RFP construct). Quantification of brightness in HeLa cells with three biological replicates reveals that FusionRed-M is \sim 2-fold brighter than FusionRed and has similar brightness to mCherry (Fig. 4b), which is the most widely used RFP.

OSER assay

Directed evolution of FusionRed generated multiple mutants that showed higher brightness in yeast (FR-F, FR-G, FR-H, FR-1) and mammalian cell lines (FR-1, FusionRed-M). Next, we

Table 2 Photo-physical properties of the mutants derived from FR-1. Brightness in mammalian (HeLa) cells presented here are the mean fluorescence intensity of the cells expressing the mutants as measured in FACS screening (Fig. 4b). λ_{abs} and λ_{em} are the maximum wavelengths of visible absorption and emission spectra, respectively. τ is the excited state lifetime. φ is the fluorescence quantum yield. ε_{max} is the extinction coefficient at the absorption peak. Details of photo-physical characterization are described in the ESI Section S11

RFP	λ_{abs} (nm)	λ_{em} (nm)	τ (ns)	φ	$\varepsilon_{\mathrm{max}} \left(\mathrm{M}^{-1} \ \mathrm{cm}^{-1} \right)$	Molecular brightness ($\varepsilon \times \varphi$)	Brightness (in HeLa)
FusionRed FR-1	575 569	596 594	1.8 2.3	0.26 0.34	87 300 84 900	100 127	100 116
FusionRed-M	571	594	2.1	0.34	71 100	107	191

investigated whether the additional mutations in FusionRed introduced any detrimental effect on its monomeric character. The in vivo dimerization tendency of FusionRed mutants was studied by performing the organized smooth endoplasmic reticulum (OSER) assay.³⁸ FPs were fused to the cytoplasmicend of the endoplasmic reticulum (ER) signal anchor membrane protein (CytERM) and expressed in HeLa cells. FPs with in vivo oligomeric tendencies tend to interact with each other, driving the restructuring of the reticular architecture of ER. This leads to the formation of OSER, which is manifested by small, bright puncta or whorls in fluorescence imaging (Fig. 5b). The OSER score, defined as the percentage of cells expressing CytERM-RFP constructs displaying no whorl, can be used to quantify the in vivo dimerization tendency, i.e. an OSER score of 100 or 0 refers to a completely monomeric or oligomeric FP, respectively.

The identification of whorls from a large number of cells is required to obtain a statistically robust OSER score. This process is tedious and subject to human bias and errors. To account for these issues, we developed a custom-based image analysis program based on CellProfiler.³⁹ Detailed description of sample preparation, image acquisition and analysis with this program are given in the ESI,† Sections S14 and S15.

Fig. 5c displays the OSER score of various RFPs as a function of the number of cells analyzed. It is evident that analysis of \sim 300 cells is sufficient to obtain a stable OSER score. Different parameters and thresholds of the image analysis program were adjusted with the known OSER score of TagRFP-T (positive control) and FusionRed (negative control). 32 As shown in Fig. 5c, TagRFP-T and FusionRed showed an OSER score of 43 and 86 respectively, which is close to the value obtained by Cranfill et al. by analyzing 10 000 cells for each FP (41.2 and 91.5 for TagRFP-T and FusionRed respectively). 32 In our hands, mCherry showed a low OSER score, in contrast with previous reports. 16,32 FusionRed and FusionRed-M showed high OSER scores indicating low in vivo oligomerization tendencies. This suggests that the increased brightness of FusionRed-M did not

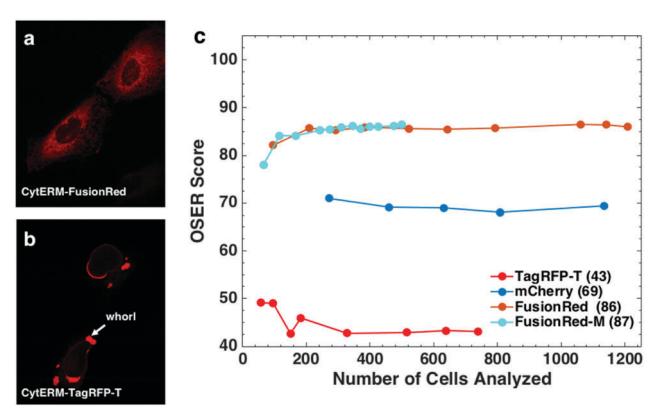


Fig. 5 OSER assay of the FusionRed mutants: (a and b) U2OS cells expressing CytERM-FusionRed and CytERM-TagRFP-T constructs. Most of the cells expressing CytERM-FusionRed constructs displayed proper localization with reticular-like structures while TagRFP-T, owing to its in vivo oligomerization tendencies, showed small (1-7 μm), bright puncta (whorls), upon fusion to CytERM. (c) OSER score of RFPs

compromise the monomeric character of FusionRed under physiological conditions.

Discussion

A microfluidic sorter capable of selecting members of cellbased FP libraries based on their excited state lifetime and fluorescence intensity has been used for the directed evolution of brightness in FusionRed. The selected mutants expressed in yeast show an improvement in lifetime and fluorescence quantum yield, resulting in higher brightness (Fig. 4a). FusionRed-M developed from the FR-1 mutant displayed ~2-fold increase in brightness upon transient expression (H2B-RFP construct) in HeLa cells (Fig. 4b). Although the molecular brightness of an FP depends only on its extinction coefficient and fluorescence quantum yield, the practical brightness in cells is a function of additional biochemical factors. For example, it depends on chromophore maturation, expression efficiency and chemical environment of the cellular compartment.⁴¹

FR-13 shows improved in vitro brightness relative to its precursor (FusionRed) due to its enhanced ε_{max} and φ . However, upon expression in yeast, FR-13 showed lower brightness. Further rounds of mutagenesis were required to improve its brightness in yeast. This result indicates that selection based on molecular photo-physical parameters such as fluorescence lifetime indeed provides the desirable improvement in molecular brightness, but it does not guarantee the brightness in cells.

Fig. 3b displays the mutations involved in the course of evolving FusionRed. The first round of mutagenesis generated FR-13 and FR-1 mutants. FR-13 contains mutations at positions 25, 49, 83 and 224 (Fig. 3b, shown in green). Photo-physical analysis of the individual FR-13 point mutants revealed that the A224T modification is responsible for its improved lifetime and quantum yield as well as its reduced in vivo brightness. The first and second rounds of mutagenesis on FR-13 introduced the modifications at position 160 (shown in purple) and positions 4, 115, 142 and 230 (shown in red), which progressively improved the brightness in yeast without affecting the lifetime. These positions are located either in loop regions or pointing out of the β-barrel. Initially, we hypothesized that mutations at these amino acid residues increase the maturation speed or enhance the expression efficiency thereby increasing the *in vivo* brightness of FR-13. However, these variants were found to have similar maturation kinetics to FR-13 in yeast (ESI,† Fig. S9). Therefore, we attribute the low brightness of FR-13 in yeast to its lower expression efficiency as estimated and compared with FusionRed and mCherry in the ESI,† Section S13. We suggest that further mutations in FR-13 have alleviated this limitation and generated FR-F, FR-G and FR-H mutants with higher brightness in yeast.

On the other hand, the FR-1 mutant displayed significant improvement upon expression in yeast. It was shown that L177M mutation was responsible for the improved lifetime and quantum yield of FR-1. The introduction of L177M

mutation in wild-type FusionRed generated the FusionRed-M mutant which displays ~2-fold higher brightness than its precursor FusionRed when expressed in mammalian cell lines. Despite the improvement in lifetime and quantum yield, FusionRed-M exhibited a reduced extinction coefficient relative to FusionRed, leading to a limited increase in molecular brightness. Therefore we attribute the enhanced brightness of FusionRed-M in mammalian cells to an improved protein expression level. As estimated in the ESI,† Section S13, the expression level of FusionRed-M is nearly 2 fold greater than that of FusionRed and 70% of that of mCherry. The improved expression level (relative to FusionRed) and higher fluorescence quantum yield (relative to mCherry) result in the brightness of FusionRed-M comparable with mCherry when expressed in mammalian cells. Though FusionRed-M was obtained by reverse engineering based on the findings from FR-1, this result suggests that if the selection was performed only based on the brightness of FACS screening, it could lead to improved brightness in cells but not necessarily at the molecular level (i.e. molecular brightness).

The OSER assay demonstrated the highly monomeric character of FusionRed-M compared to mCherry, the most widely used RFP. Depending on the biological application of RFP tools, when the monomeric character of RFPs becomes a crucial criterion, FusionRed-M may be a good substitution for mCherry or other RFPs with less or poor monomeric character.

Brightness is not the only photo-physical property of importance in fluorescence imaging. The ability to select based on complex criteria such as photostability, chromophore maturation and photoswitching will play an important role in the development of new FPs. We previously demonstrated that the measurement of photostability can also be implemented in a microfluidic sorter, enabling the selection of FP mutants with reduced photobleaching, though at the expense of reduced fluorescence lifetime and brightness.³⁰ In the current sorting system, an additional blue excitation laser can also be incorporated to monitor the completeness of chromophore formation and thereby eliminate immature RFP mutants with green emission.42 We also reported a frequency-domain approach for quantifying dark-state conversion (DSC) kinetics in FPs. 43 This technique can also be employed in a flow system for selections to generate photostable or photo-switchable FPs. When incorporated with multiple photo-physical parameters, we expect that this microfluidic system could be used to gain a better and more comprehensive understanding of the fitness landscape of FPs. This is essential for the overall development of FPs for broader utility in imaging applications.

Conclusions

We have presented a microfluidic sorter that can be utilized to select mutants from fluorescent protein libraries based on their excited state lifetime and fluorescence intensity, and visualize the trajectory of FP evolution. We demonstrated its ability by engineering variants of the FusionRed RFP with improved photophysical properties. With multiple rounds of error-prone

mutagenesis and sorting based on fluorescence lifetime and intensity, a set of mutants is generated with a significant improvement in lifetime. This enhancement of lifetime results in an increase in fluorescence quantum yield and more than 2-fold improvement in theoretical brightness (extinction coefficient x quantum yield) of the FPs. The mutants displayed significantly higher brightness in yeast relative to their precursor. A single mutation (L177M) in FusionRed enhanced its brightness by \sim 2-fold as evidenced by mammalian cell expression. Quantification of in vivo dimerization propensity of the mutants indicates that the improvement in brightness is achieved without sacrificing the monomeric character of FusionRed. At different phases of the evolution process, mutants are isolated and their photo-physical/bio-chemical properties are quantified. This enables us to visualize the trajectory of directed evolution in FusionRed. Mutations associated with error-prone mutagenesis have been discussed in the context of their role in modifying the lifetime, maturation speed and expression efficiency. These investigations revealed that directed evolution on fluorescence lifetime is capable of achieving improvements in brightness within a specific host organism. Fortunately, microfluidic sorting is compatible with a wide range of cells and organisms such as bacteria, yeast, mammalian and plant cells. Furthermore, the microfluidic sorter can be modified to incorporate other photo-physical parameters, e.g. photostability, dark state conversion etc. This will be useful for simultaneous improvement and monitoring of multiple essential photo-physical properties of FPs and has the potential for a more comprehensive understanding of their fitness landscapes.

Conflicts of interest

There are no conflicts of interest to declare.

Acknowledgements

This work was supported by the NSF Physics Frontier Center at JILA (PHY 1734006 to R. J.) and NIH DP1 GM114863 and R01 GM084027 (to A. E. P.). RJ is a staff member in the Quantum Physics Division of the National Institute of Standards and Technology (NIST). Certain commercial equipment, instruments, or materials are identified in this paper in order to specify the experimental procedure adequately. Such identification is not intended to imply recommendation or endorsement by the NIST, nor is it intended to imply that the materials or equipment identified are necessarily the best available for the purpose. We acknowledge the Flow Cytometry facility at BioFrontiers Institute, CU Boulder (supported by NIH S10ODO21601). The imaging work was performed at the BioFrontiers Institute Advanced Light Microscopy Core. Spinning disc confocal microscopy was performed on a Nikon Ti-E microscope supported by the BioFrontiers Institute and the Howard Hughes Medical Institute. We thank Dr Joe Dragavon for helpful discussion on confocal imaging. Fluorescence measurements were performed at Biochemistry Shared Instruments Pool. The absorption measurement was

performed at JILA Keck Laboratory. Structure figures were made with VMD, which was developed by the Theoretical and Computational Biophysics Group in the Beckman Institute for Advanced Science and Technology at the University of Illinois at Urbana-Champaign.

References

- 1 E. A. Rodriguez, R. E. Campbell, J. Y. Lin, M. Z. Lin, A. Miyawaki, A. E. Palmer, X. K. Shu, J. Zhang and R. Y. Tsien, Trends Biochem. Sci., 2017, 42, 111-129.
- 2 S. Waldchen, J. Lehmann, T. Klein, S. van de Linde and M. Sauer, Sci. Rep., 2015, 5, 15348.
- 3 E. A. Rodriguez, G. N. Tran, L. A. Gross, J. L. Crisp, X. K. Shu, J. Y. Lin and R. Y. Tsien, Nat. Methods, 2016, 13, 763-769.
- 4 G. Matela, P. Gao, G. Guigas, A. F. Eckert, K. Nienhaus and G. U. Nienhaus, Chem. Commun., 2017, 53, 979-982.
- 5 K. D. Piatkevich, V. N. Malashkevich, K. S. Morozova, N. A. Nemkovich, S. C. Almo and V. V. Verkhusha, Sci. Rep., 2013, 3, 1847.
- 6 J. Chu, R. D. Haynes, S. Y. Corbel, P. P. Li, E. Gonzalez-Gonzalez, J. S. Burg, N. J. Ataie, A. J. Lam, P. J. Cranfill, M. A. Baird, M. W. Davidson, H. L. Ng, K. C. Garcia, C. H. Contag, K. Shen, H. M. Blau and M. Z. Lin, Nat. Methods, 2014, 11, 572-578.
- 7 N. C. Shaner, R. E. Campbell, P. A. Steinbach, B. N. G. Giepmans, A. E. Palmer and R. Y. Tsien, Nat. Biotechnol., 2004, 22, 1567-1572.
- 8 N. C. Shaner, M. Z. Lin, M. R. McKeown, P. A. Steinbach, K. L. Hazelwood, M. W. Davidson and R. Y. Tsien, Nat. Methods, 2008, 5, 545-551.
- 9 I. I. Shemiakina, G. V. Ermakova, P. J. Cranfill, M. A. Baird, R. A. Evans, E. A. Souslova, D. B. Staroverov, A. Y. Gorokhovatsky, E. V. Putintseva, T. V. Gorodnicheva, T. V. Chepurnykh, L. Strukova, S. Lukyanov, A. G. Zaraisky, M. W. Davidson, D. M. Chudakov and D. Shcherbo, Nat. Commun., 2012, 3, 1204.
- 10 Y.-T. Kao, X. Zhu and W. Min, Proc. Natl. Acad. Sci. U. S. A., 2012, 109, 3220-3225.
- 11 J. Goedhart, D. von Stetten, M. Noirclerc-Savoye, M. Lelimousin, L. Joosen, M. A. Hink, L. van Weeren, T. W. J. Gadella and A. Royant, Nat. Commun., 2012, 3, 751.
- 12 E. M. Merzlyak, J. Goedhart, D. Shcherbo, M. E. Bulina, A. S. Shcheglov, A. F. Fradkov, A. Gaintzeva, K. A. Lukyanov, S. Lukyanov, T. W. J. Gadella and D. M. Chudakov, Nat. Methods, 2007, 4, 555-557.
- 13 H. Mizuno, P. Dedecker, R. Ando, T. Fukano, J. Hofkens and A. Miyawaki, Photochem. Photobiol. Sci., 2010, 9, 239-248.
- 14 S. Duwe, E. De Zitter, V. Gielen, B. Moeyaert, W. Vandenberg, T. Grotjohann, K. Clays, S. Jakobs, L. Van Meervelt and P. Dedecker, ACS Nano, 2015, 9, 9528-9541.
- 15 J. Goedhart, L. van Weeren, M. A. Hink, N. O. E. Vischer, K. Jalink and T. W. J. Gadella, Nat. Methods, 2010, 7, 137-139.
- 16 D. S. Bindels, L. Haarbosch, L. van Weeren, M. Postma, K. E. Wieser, M. Mastop, S. Aumonier, G. Gotthard,

- A. Royant, M. A. Hink and T. W. J. Gadella, Nat. Methods, 2017, 14, 53-56.
- 17 K. P. Carter, M. C. Carpenter, B. Fiedler, R. Jimenez and A. E. Palmer, Anal. Chem., 2017, 89, 9601-9608.
- 18 N. B. Arnfinnsdottir, A. V. Bjorkoy, R. Lale and M. Sletmoen, RSC Adv., 2016, 6, 36198-36206.
- 19 L. Wang, W. C. Jackson, P. A. Steinbach and R. Y. Tsien, Proc. Natl. Acad. Sci. U. S. A., 2004, 101, 16745-16749.
- 20 J. Nedbal, V. Visitkul, E. Ortiz-Zapater, G. Weitsman, P. Chana, D. R. Matthews, T. Ng and S. M. Ameer-Beg, Cytometry, Part A, 2015, 87a, 104-118.
- 21 B. G. Pinsky, J. J. Ladasky, J. R. Lakowicz, K. Berndt and R. A. Hoffman, Cytometry, 1993, 14, 123-135.
- 22 J. A. Steinkamp and H. A. Crissman, Cytometry, 1993, 14, 210-216.
- 23 C. Deka, B. E. Lehnert, N. M. Lehnert, G. M. Jones, L. A. Sklar and J. A. Steinkamp, Cytometry, 1996, 25, 271-279.
- 24 H. H. Cui, J. G. Valdez, J. A. Steinkamp and H. A. Crissman, Cytometry, Part A, 2003, 52a, 46-55.
- 25 R. Cao, V. Pankayatselvan and J. P. Houston, Opt. Express, 2013, 21, 14816-14831.
- 26 J. P. Houston, M. A. Naivar and J. P. Freyer, Cytometry, Part A, 2010, 77a, 861-872.
- 27 B. Sands, P. Jenkins, W. J. Peria, M. Naivar, J. P. Houston and R. Brent, PLoS One, 2014, 9, e109940.
- 28 Z. H. Yang, D. M. Shcherbakova, V. V. Verkhusha and J. P. Houston Conference on Lasers and Electro-Optics (Cleo), 2016, (1-3).
- 29 L. M. Davis, J. L. Lubbeck, K. M. Dean, A. E. Palmer and R. Jimenez, Lab Chip, 2013, 13, 2320-2327.
- 30 K. M. Dean, J. L. Lubbeck, L. M. Davis, C. K. Regmi, P. P. Chapagain, B. S. Gerstman, R. Jimenez and A. E. Palmer, Integr. Biol., 2015, 7, 263-273.
- 31 K. M. Dean, L. M. Davis, J. L. Lubbeck, P. Manna, P. Friis, A. E. Palmer and R. Jimenez, Anal. Chem., 2015, 87, 5026-5030.
- 32 P. J. Cranfill, B. R. Sell, M. A. Baird, J. R. Allen, Z. Lavagnino, H. M. de Gruiter, G. J. Kremers, M. W. Davidson, A. Ustione and D. W. Piston, Nat. Methods, 2016, 13, 557-562.
- 33 J. L. Lubbeck, K. M. Dean, H. Ma, A. E. Palmer and R. Jimenez, Anal. Chem., 2012, 84, 3929-3937.
- 34 W. M. Patrick, A. E. Firth and J. M. Blackburn, *Protein Eng.*, 2003, 16, 451-457.
- 35 K. D. Piatkevich, E. E. Jung, C. Straub, C. Y. Linghu, D. Park, H. J. Suk, D. R. Hochbaum, D. Goodwin, E. Pnevmatikakis, N. Pak, T. Kawashima, C. T. Yang, J. L. Rhoades, O. Shemesh, S. Asano, Y. G. Yoon, L. Freifeld, J. L. Saulnier, C. Riegler, F. Engert, T. Hughes, M. Drobizhev, B. Szabo, M. B. Ahrens, S. W. Flavell, B. L. Sabatini and E. S. Boyden, Nat. Chem. Biol., 2018, 14, 352-360.
- 36 D. Shcherbo, C. S. Murphy, G. V. Ermakova, E. A. Solovieva, T. V. Chepurnykh, A. S. Shcheglov, V. V. Verkhusha, V. Z. Pletnev, K. L. Hazelwood, P. M. Roche, S. Lukyanov, A. G. Zaraisky, M. W. Davidson and D. M. Chudakov, Biochem. J., 2009, 418, 567-574.
- 37 W. L. Noderer, R. J. Flockhart, A. Bhaduri, A. J. D. de Arce, J. J. Zhang, P. A. Khavari and C. L. Wang, Mol. Syst. Biol., 2014, 10, 748.

38 L. M. Costantini, M. Fossati, M. Francolini and E. L. Snapp, Traffic, 2012, 13, 643-649.

- 39 L. Kamentsky, T. R. Jones, A. Fraser, M. A. Bray, D. J. Logan, K. L. Madden, V. Ljosa, C. Rueden, K. W. Eliceiri and A. E. Carpenter, Bioinformatics, 2011, 27, 1179-1180.
- 40 W. Humphrey, A. Dalke and K. Schulten, J. Mol. Graphics Modell., 1996, 14, 33-38.
- 41 E. Balleza, J. M. Kim and P. Cluzel, Nat. Methods, 2018, 15, 47-51.
- 42 K. B. Bravaya, O. M. Subach, N. Korovina, V. V. Verkhusha and A. I. Krylov, J. Am. Chem. Soc., 2012, 134, 2807-2814.
- 43 P. Manna and R. Jimenez, J. Phys. Chem. B, 2015, 119, 4944-4954.